

Microdroplet splitting and mixing by portable triboelectric nanogenerator

Qi Gao^{1,3,§}, Qin Xiang^{3,4,§}, Wenkai Liu^{3,§}, Mengru Ding³, Wei Long⁴, Jianlong Wang³, Xiaojun Cheng^{1,3}, Hengyu Li^{1,2,3}, Zhong Lin Wang^{1,3}, and Tinghai Cheng^{1,3}

¹ Guangzhou Institute of Blue Energy, Knowledge City, Huangpu District, Guangzhou 510555, China

² State Key Laboratory of Fluid Power and Mechatronic Systems, Zhejiang University, Hangzhou 310027, China

³ Beijing Institute of Nanoenergy and Nanosystems, Chinese Academy of Sciences, Beijing 101400, China

⁴ Faculty of Mechanical and Electrical Engineering, Kunming University of Science and Technology, Kunming 650500, China

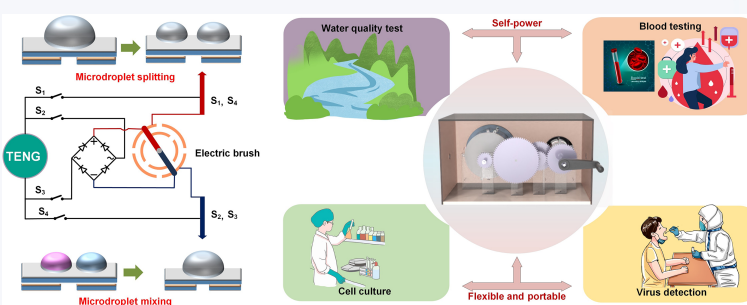
[§] Qi Gao, Qin Xiang, and Wenkai Liu contributed equally to this work.



Cite this article: *Nano Research*, 2025, 18, 94907128. <https://doi.org/10.26599/NR.2025.94907128>

ABSTRACT: The advancement of digital microfluidics technology has been pivotal in academic research and engineering applications. However, the prevailing limitation is that traditional voltage sources generate an excess of Joule heat, adversely impacting droplet operation. Moreover, the power supply equipment required by digital microfluidics limits its applications. Here, we propose a self-powered microdroplet manipulation (SMDM) via triboelectric nanogenerator (TENG), which presents a capability for splitting and mixing different kinds of droplets. Fundamentally, SMDM is based on the electroosmotic flow principle, thereby enabling droplet splitting in the range of from 2 to 630 μL . Notably, for droplet splitting in the range of from 5 to 60 μL , the TENG only requires a power output ranging from 2.704 to 6.084 mW. In addition, SMDM demonstrates proficiency in droplet mixing, which achieves complete mixing of 10 μL droplets in 60 s and 30 μL droplets in a mere 53 s. Therefore, leveraging the strengths of the TENG, a self-powered microdroplet manipulated system is designed for digital microfluidics. It carries significant advantages over the traditional voltage source, including self-powered, low-Joule heat, increased safety and enhanced portability. This research provides a new solution for portable applications of digital microfluidics.

KEYWORDS: triboelectric nanogenerator, microdroplet manipulation, digital microfluidics, droplet splitting, droplet mixing



1 Introduction

Digital microfluidics, a significant subfield of microfluidics, possesses the vast potential for varied applications across multiple industries [1–6]. Within microfluidics, the ability to splitting and mixing droplets is vital, enabling effective droplet manipulation and reactions [7–10]. Droplet splitting facilitates the sample partitioning and analysis by reducing volumes, while droplet mixing initiates and expedites reactions through the amalgamation of several

chemicals. Several techniques are currently being used for droplet splitting and mixing, including electric field [11–14], ultrasonic field [15, 16], magnetic field [17, 18], etc. Among these, the electric field technique offers significant advantages due to its capacity for precise manipulation. The strength and direction of the electric field can be adjusted to control the shape [12], size [19] and position [20] of the droplet, making it a popular choice in digital microfluidics. Combined with artificial intelligence, the versatility and application performance of digital microfluidics are further improved [21, 22]. However, traditional voltage sources are usually bulky and require additional equipment such as signal generators and power amplifiers, making them unsuitable for miniaturized and portable applications [23–26]. Furthermore, their high energy consumption and resultant heat generation can negatively impact droplet operation, affecting its stability and effectiveness. Additionally, these sources require an external power supply, further limiting their applicability. Because of these limitations, there is an urgent need

Received: August 11, 2024; Revised: October 21, 2024

Accepted: November 13, 2024

✉ Address correspondence to Hengyu Li, lihengyu@binn.cas.cn; Zhong Lin Wang, zhong.wang@mse.gatech.edu; Tinghai Cheng, chengtinghai@binn.cas.cn

for a new portable, safe and controllable microdroplet operation technology.

The triboelectric nanogenerator (TENG) [27], is an emerging technology proposed by Professor Zhong Lin Wang in 2012. It excites the intermolecular action within the material and between the material interfaces and expresses the effect of the action caused by the change of energy between molecules in the form of electrical signals. This makes it simple, easy to manufacture, portable [28], etc., which is widely used in plasma production [29–33], droplet manipulation and microfluidics [34–37], sensing [38–42] and wearable devices [43, 44], owing to its distinct characteristics of high voltage output and low current [45]. In the field of microfluidics, utilizing TENG as a source of voltage has a significant advantage over the traditional voltage source. Droplet microfluidic technology can enable high-throughput analysis and experiments, but more efficient methods and equipment are still needed for large-scale, precisely controlled droplet manipulation [46]. There are still many problems in the processing of complex samples, such as the composition of complex, easy to cause corrosion to the manipulation platform. The complex composition of the droplet leads to complex properties and behaviors of the droplet [47, 48]. At present, some scholars have applied TENG to the operation of continuous fluid in microfluidic chips. Some scholars also realize long-distance droplet transport through the high-pressure characteristics of TENG [49]. Therefore, finding an alternative solution for digital microfluidics by utilizing TENG high voltage to change the contact angle between liquids and solids can effectively solve the limitations of traditional droplet splitting and mixing techniques.

Herein, we propose a self-powered microdroplet manipulation (SMDM) via the TENG. Using TENG based on freestanding triboelectric-layer mode as a high voltage source to drive droplets. The electric brush is used to conduct voltage and current between the TENG and the microdroplet manipulation platform, primarily to control the direction of the electric field force on the droplet. Fundamentally, the SMDM manipulates on the principle of electroosmotic flow, which enables droplet splitting. The SMDM also has unique advantages in droplet mixing, providing a new solution to the common cross-contamination problem existing in traditional solution mixing. Leveraging the high-voltage properties of TENG, a self-powered microdroplet manipulated system is developed based on SMDM, offering notable benefits over traditional voltage sources, including reduced power consumption, enhanced safety and improved portability. This portable self-powered microdroplet manipulated system is poised to serve a vital function in water quality testing, cell culture, blood testing and virus detection. This advancement is likely to promote the commercialization of digital microfluidics.

2 Results and discussion

2.1 Concepts of SMDM

As depicted in Fig. 1(a), digital microfluidics technology plays a pivotal role across diverse sectors, encompassing biology [50, 51], chemistry [52, 53] and environmental studies [54, 55]. Primarily manipulated by electric field, traditional digital microfluidics, however, confronts several limitations like bulkiness and high-

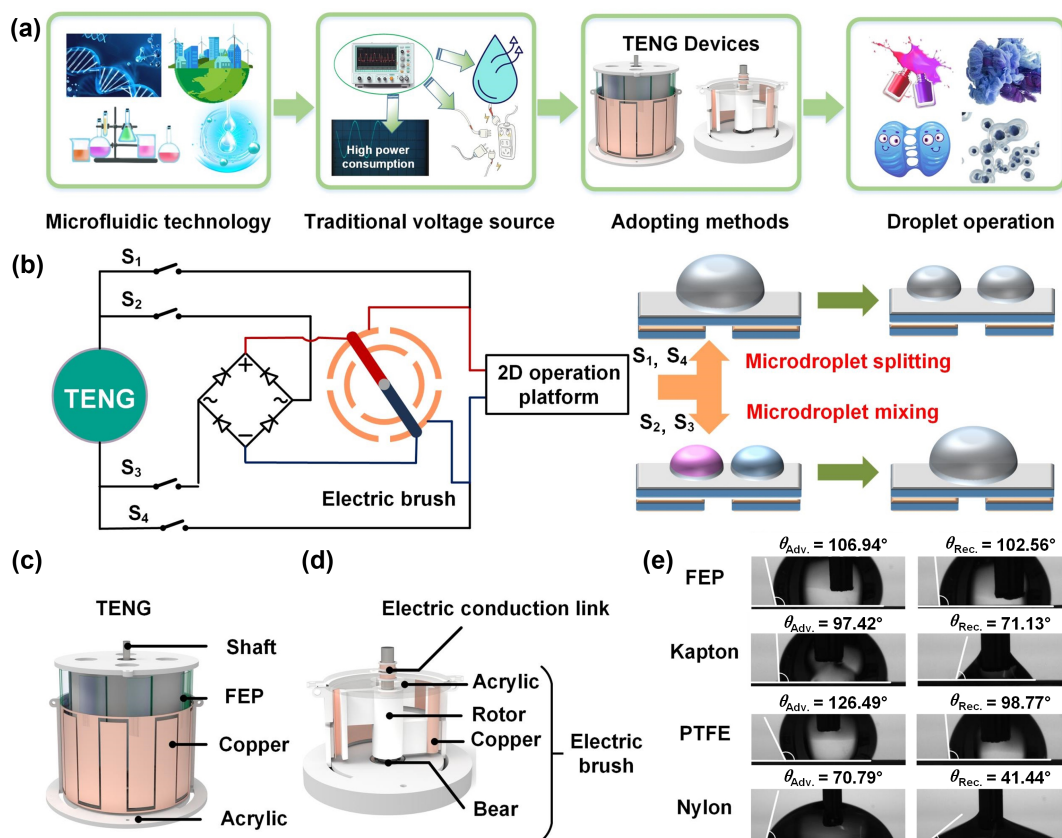


Figure 1 The SMDM concepts. (a) Conceptual diagram of microdroplet operation. (b) Schematic diagram of the SMDM execution structure. (c) TENG structure diagram. (d) Electric brush structure diagram. (e) Advancing and receding contact angles of different materials with deionized water.

power consumption, making it less viable for miniaturized and portable applications. In contrast, our work proposes an SMDM based on the TENG that more appropriately caters to microdroplet operation requirements due to enhanced control and safety. The comprehensive structure of the SMDM is schematically presented in Fig. 1(b). The TENG is employed as a voltage source, which enables varied droplet operations in conjunction with circuit-switching and the addition of an electric brush. Figure 1(c) shows a TENG consisting of a rotor plus fluorinated ethylene propylene (FEP) film toggles plus copper. Figure 1(d) shows the brushes consisting of conductive slip rings and rotating tabs. When the switches S_1 and S_4 are engaged, the output voltage generated by the TENG directly interfaces with the microfluidics platform, triggering droplet splitting. Conversely, when switches S_2 and S_3 are engaged, the TENG's output voltage connects to the conductive slip ring via a rectifier bridge. The electric brush distributes the voltage to various microfluidics electrodes, causing the droplets to undergo alternating forces under the electric field, thereby facilitating droplet mixing.

To achieve meticulous control of droplets, it is crucial to minimize the force affecting their motion on the plane. On an imperfect contact surface, both the droplet and the material with which it interacts exhibit a peak advancing contact angle and a trough receding contact angle. The discrepancy between these two

angles reflects the magnitude of the frictional resistance exerted on the droplet moving along the plane, termed contact angle hysteresis, as illustrated in Fig. 1(e). In this experiment, several common hydrophobic materials, namely FEP, Kapton, polytetrafluoroethylene (PTFE) and Nylon are selected for consideration as films. The contact angle hysteresis values for these materials were measured to be 4.38°, 26.29°, 27.72° and 29.35°, respectively. The FEP film exhibits the smallest contact angle hysteresis, which means that the frictional resistance encountered by the droplet in contact with this material is minimal. As such, the FEP film is selected as the experimental material for microdroplet operations in subsequent experiments.

2.2 Principle of SMDM

The SMDM primarily comprises the TENG, an electric brush and a microdroplet manipulation platform. Initially, a freestanding TENG manipulating in a rotary mode is employed as the voltage source. When the copper and FEP film come into contact, electrons from the copper electrode transfer to the FEP film, creating a positive charge on the copper electrode and a negative charge on the FEP film. Upon connecting an external electrometer to the TENG, the potential difference induces electron flow in the circuit, generating the current. This potential difference disappears when the relative motion between the copper electrode and the FEP film ceases,

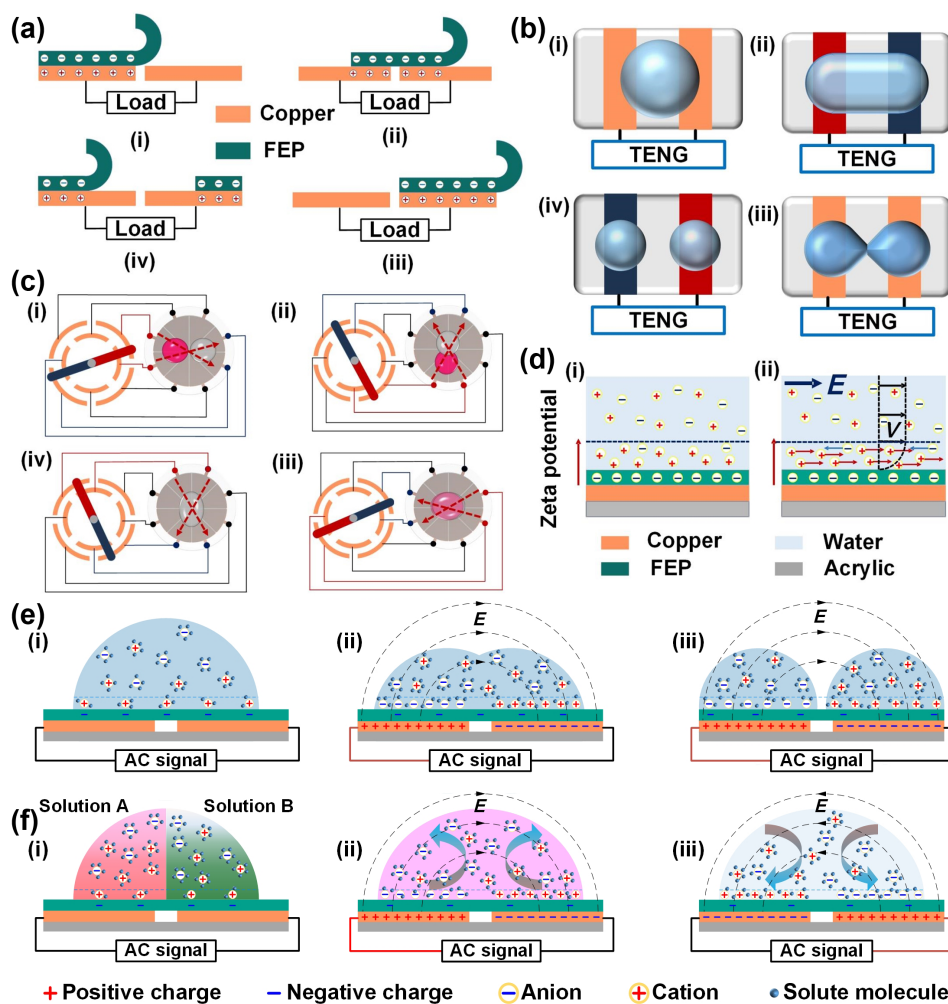


Figure 2 Schematic diagram of SMDM. (a) Working principles diagram of TENG. (b) Diagram of droplet division. (c) Electric brush working principles diagram. (d) Alternating current penetration. (e) AC electroosmotic splitting mechanism diagram. (f) AC electroosmotic mixing mechanism diagram.

prompting the next signal cycle with subsequent friction, as depicted in Fig. 2(a). When the voltage produced by the TENG is applied directly to the droplet connected to the microdroplet manipulation platform, the droplet splitting occurs, as demonstrated in Fig. 2(b). If the voltage generated by the TENG is relayed to the conductive slip ring and electric brush via the rectifier bridge, the continual rotation of the brush sheet enables the microdroplets to undergo alternating forces in different directions, thereby promoting droplet mixing, as shown in Fig. 2(c).

The fundamental principle for driving droplet motion via an electric field is the electroosmotic flow. On a macroscopic scale, when a droplet is placed on an FEP film, the film adsorbs positively charged counter ions from the solution to preserve local electrical neutrality. This process results in an induced double layer on the FEP film due to the internal charge distribution of the droplet, as shown in Fig. 2(d)(i). When the droplet is subject to the electric field force produced by the TENG, the fused double layer is propelled by Coulomb forces, carrying the adjacent liquid along and causing the solution to move directionally at a consistent speed, as illustrated in Fig. 2(d)(ii).

If the TENG electric field direction consistently alternates in a single direction, on a microscopic level, the cation carries the solute molecule moving in the opposite direction of the electric field line and the anion carries the solute molecule moving in the direction of the electric field line. Finally, the droplet is “torn” into two droplets in the repeated motion driven by the alternating electric field, as demonstrated in Fig. 2(e). However, if the electric field’s direction is

continuously changing spatially, the ions within the liquid will not move consistently in one direction, but instead shift with the electric field’s direction. As the direction of the electric field continually changes, two alternating positive/negative “vortices” are generated within the droplet, as shown in Fig. 2(f). After several “vortex” alternations, droplet mixing is achieved.

2.3 TENG output performance

To evaluate the output performance of the TENG, it is directly connected to an electrometer, as depicted in Fig. 3(a)(i). Figures 3(a)(ii) and 3(a)(iii) shows the effect of different rotational speeds on the TENG open-circuit voltage and short-circuit current. As the rotational speed elevates from 50 to 300 r·min⁻¹, the open-circuit voltage (V_{OC}) escalates from 0.8 to 1.9 kV and the short-circuit current (I_{SC}) surges from 6 to 25 μ A. Conversely, the output performance of the electric brush is assessed after the rectifier bridge, with the measurement circuit diagram illustrated in Fig. 3(b)(i). As indicated in Figs. 3(b)(ii) and 3(b)(iii), the open-circuit voltage of the electric brush rises from 0.35 to 0.75 kV as the speed augments from 50 to 300 r·min⁻¹, while the short-circuit current remains consistent.

In order to verify whether the output performance of TENG is affected by droplet operation after long-term operation. Durability experiments were conducted on the TENG, the specific structure of which is shown in Fig. S1(a) in the Electronic Supplementary Material (ESM). The rotational speed of the TENG was selected to be 150 r·min⁻¹ during the test, as shown in Fig. S1(b) in the ESM.

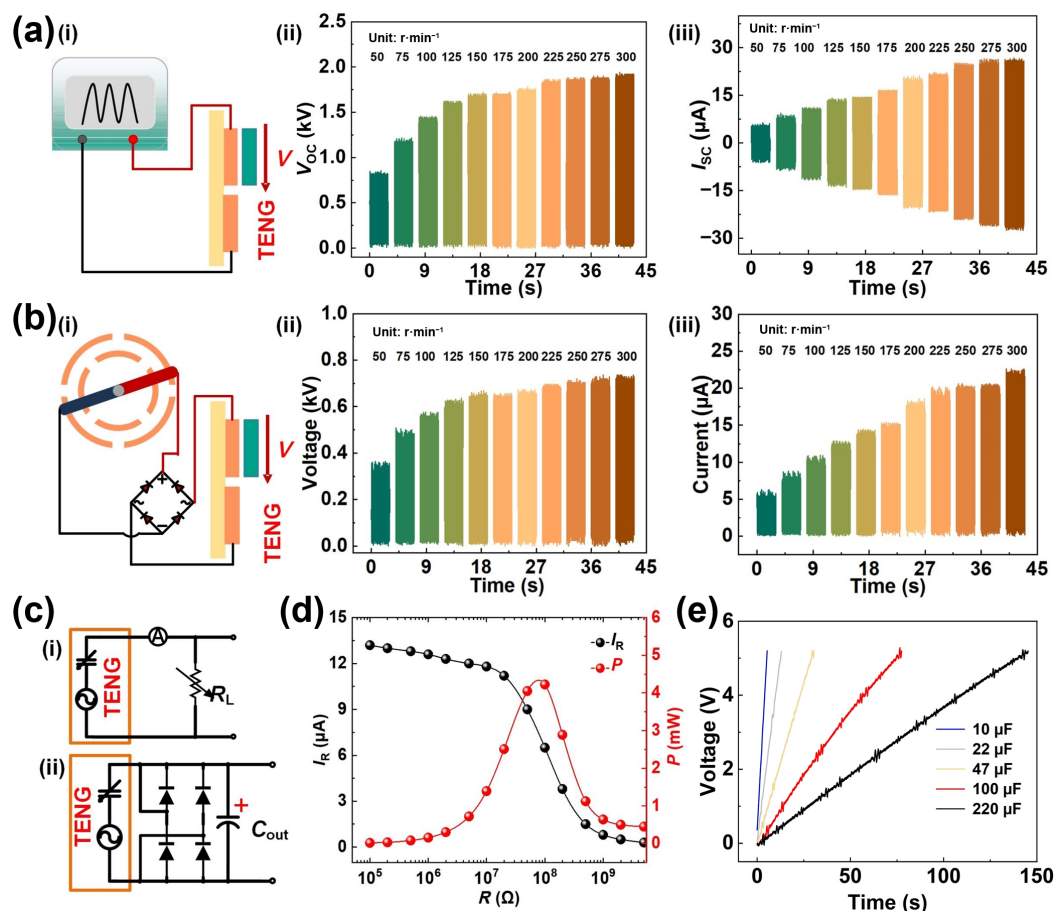


Figure 3 Output performance test of TENG. (a) Basic output of the TENG. (b) Basic output of the electric brush. (c) Power measurement diagram (i) and charge capacity diagram (ii) of the TENG. (d) Power curve. (e) Charge capacity curve.

The TENG was operated for 8×10^4 cycles. After 8×10^4 cycles, the output short-circuit current of TENG decreased slightly. This is shown in Figs. S1(b)(i) and S1(b)(ii) in the ESM.

Subsequently, the other output performances of the TENG are tested according to the power measurement circuit diagrams and charging capacitance circuit diagrams provided in Fig. 3(c), where R_L denotes the variable resistance and C_{out} denotes the output capacitance.

The rotational speed of TENG is maintained at $180 \text{ r}\cdot\text{min}^{-1}$. The outcomes from the experiment indicate that the current under external load (I_R) of the TENG decreases with the increase of the matched impedance. Furthermore, the TENG's peak power (P) exhibits a pattern of growth followed by reduction, suggesting that the ideal matching impedance for the TENG's power output is $100 \text{ M}\Omega$, depicted in Fig. 3(d). The TENG's optimal power output is 4.225 mW . Charging a capacitor using TENG takes only 5.3 s to reach 5 V for a $10 \text{ }\mu\text{F}$ capacitor and 145 s for a $220 \text{ }\mu\text{F}$ capacitor, as demonstrated in Fig. 3(e). In a word, the TENG shows excellent performance in microdroplet operation.

2.4 The SMDM control droplet splitting

Figure 4(a) demonstrates the droplet splitting force based on

SMDM. The droplet is subjected to gravity (G), plane support force (F), and Coulomb forces from adjacent electrodes (F_1 and F_2). When an alternating current (AC) electric field is applied on either side of the droplet, the electrons within the droplet migrate in the direction opposing the electric field, thereby creating a "tearing" force on the droplet that results in its splitting. To examine the impact of SMDM on droplet splitting, we first vary the size of the microdroplet manipulation platform. The changes are investigated in the volume range of the splitting droplet as a function of the electrode broad (E_B) and electrode gap (E_G), illustrated in Fig. S2(a) in the ESM. The experimental findings reveal that as E_B and E_G augment from 2 to 8 mm , the minimum droplet volume required for splitting enlarges from 2 to $130 \text{ }\mu\text{L}$; and the maximum droplet volume that can be split expands from 5 to $630 \text{ }\mu\text{L}$, as depicted in Fig. 4(b). Given that droplet splitting necessitates partial coverage of the electrode area by the droplet, the minimum volume of the droplet primarily depends on the E_G and increases as the E_G expands. Once the droplet is "torn" beyond the two electrodes, it cannot be lifted any further. The maximum volume that can be split is predominantly contingent on the total width of the E_B and E_G and this maximum volume escalates with the total broad.

However, droplet manipulation often encounters multiple

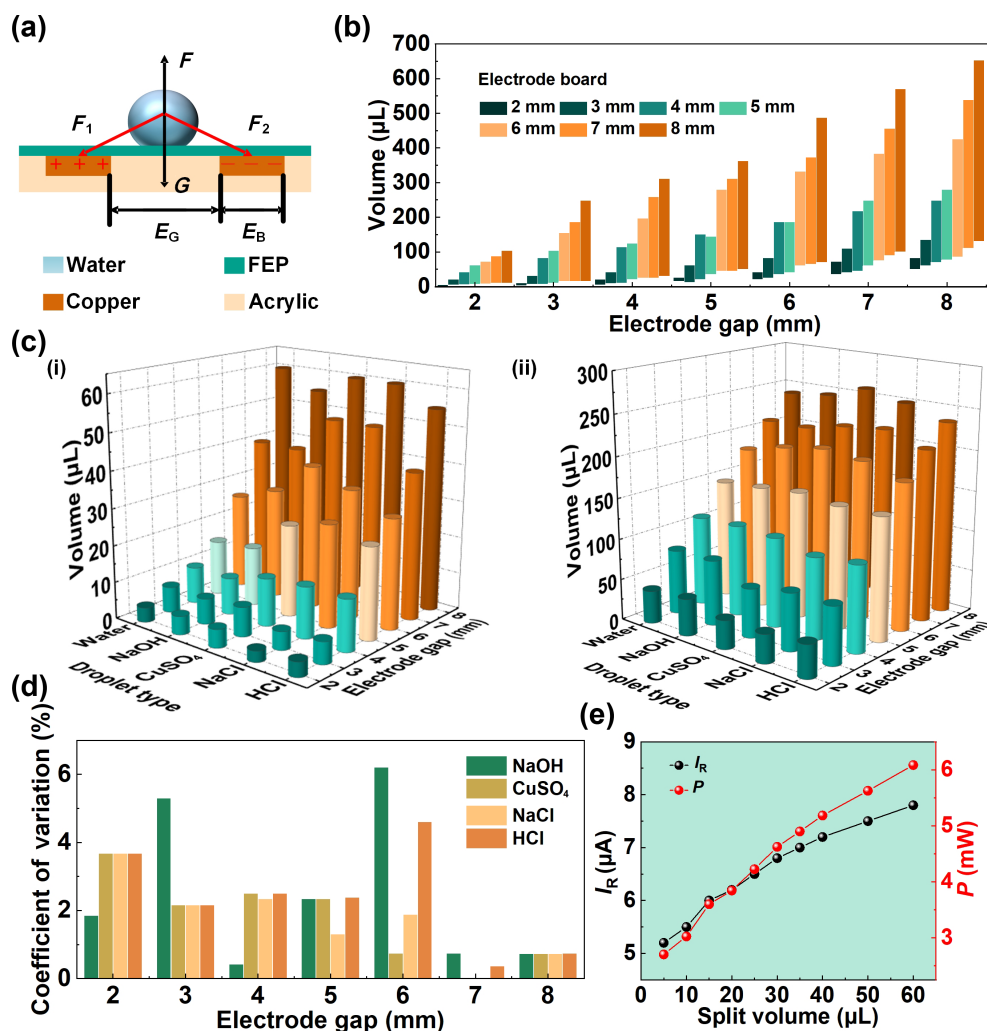


Figure 4 Droplet splitting control using SMDM. (a) Schematic diagram of droplet splitting structure. (b) Relationship between the minimum and maximum volume of split droplets and electrode gap and broad. (c) The minimum and maximum volume of different kinds of droplets varies with the electrode gap. (d) Coefficient of open circuit voltage variation required for different droplet splitting. (e) Output power of TENG splitting different volume droplets.

chemical reactions, so the capability to split various types of droplets remains a crucial parameter. Keeping the E_B fixed at 4 mm and varying the E_C from 2 to 8 mm, we obtain the splitting results for different types of droplets (NaOH, CuSO_4 , NaCl, HCl) as shown in Figs. 4(c)(i) and 4(c)(ii). For an E_C of 2 mm, the device can split a minimum volume of 3 μL of a NaCl solution and a maximum volume of 45 μL of a NaOH solution; for an E_C of 8 mm, it can split a minimum volume of 55 μL of NaOH and HCl solution and a maximum volume of 260 μL of a CuSO_4 solution.

These results suggest that the TENG can split droplets of different volumes independent of the species and the voltage difference required for splitting various types of droplets does not exceed 0.16 kV, as indicated in Fig. S2(b) in the ESM, according to Eq. (1)

$$CV = \frac{SD}{MN} \times 100\% \quad (1)$$

where CV, SD and MN denote the coefficient of variation, standard deviation and mean of value.

The coefficients of variation are obtained in Fig. 4(d), where the maximum coefficient of variation is 6.3%. The output voltage required to splitting different volumes of droplets from the TENG is measured against the matched impedance obtained from the

peak power of the TENG. The power consumption required by TENG to splitting droplets with different volumes is obtained and shown in Fig. 4(e). The power consumption required for splitting droplets based on TENG is much lower than that of conventional voltage [19]. This gives it a more advanced edge in digital microfluidics.

2.5 The SMDM to control droplet mixing

The SMDM is capable of efficiently executing specific chemical reactions within droplets on an open two-dimensional plane, which is accomplished by connecting the TENG to the electrodes of the microdroplet manipulation platform via an electric brush.

Figure 5(a) presents the finite element calculation results of the electric coalescence phenomenon, simulated in software COMSOL, involving two droplets situated in an electric field environment with an applied voltage of 1.5 kV. During the mixing of droplets, initially, the velocities inside the droplets all orient in a single direction, as depicted in Fig. 5(b)(i). As the direction of the electric field force alters, the velocity direction inside the droplet becomes opposite to the initial direction of the force, resulting in a “vortex” phenomenon at the juncture where the velocity changes its direction within the droplet, as illustrated in Fig. 5(b)(ii). This “vortex” phenomenon dissipates once the internal velocity direction

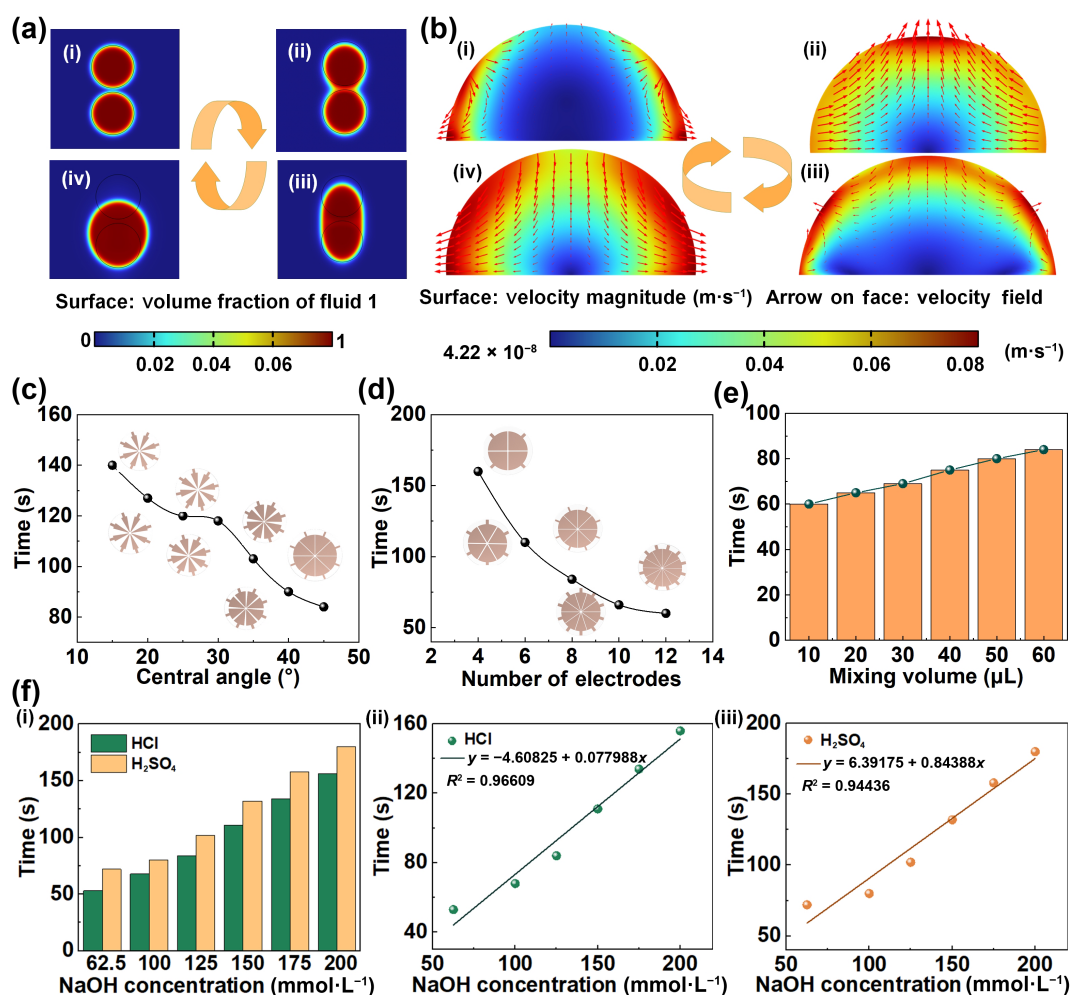


Figure 5 Performance of self-powered hybrid SMDM. (a) Droplet mixing process under the action of electric field force. (b) Changing process of the velocity field inside the droplet. (c) Interrelation between the duration of mixing and center angle. (d) Interrelation between the duration of mixing and the count of electrodes. (e) Interrelation between the duration of mixing and droplet volume. (f) Interrelation between mixing duration, concentration and droplet type.

of the droplet aligns with the force direction of the electric field, as demonstrated in Fig. 5(b)(iii). Upon the next change in the electric field direction, the force inside the droplet again opposes the velocity direction, triggering a second “vortex” phenomenon. This “vortex” rotates in a direction opposite to the initial “vortex”, as shown in Fig. 5(b)(iv). After undergoing this cyclic process, the droplets achieve a mixed state over a period.

To explore the impact of the SMDM on microdroplet mixing time, we conducted experiments using 125 mmol·L⁻¹ solutions of NaOH and HCl, as depicted in Fig. S3(a) in the ESM. Initially, without any additional auxiliary devices, it takes 420 s to complete the mixing of two 30 μL droplets. However, when we applied an electric field force to the droplets, the droplet mixing time is significantly decreased. First, we modified the central angle of the electrode on the microdroplet manipulation platform, with various central angle electrodes illustrated in Fig. S3(b) in the ESM. As shown in Fig. 5(c), when the electrode central angle is increase from 15° to 45°, the droplet mixing time decrease from 140 to 84 s. This can be attributed to the fact that with an increasing electrode central angle, the electrode area in contact with the droplet enlarges, thereby raising the number of ions subjected to the electric field force per unit area, thus enhancing the droplet mixing efficiency. Figure 5(d) explores the correlation between the number of electrodes and droplet mixing time, with its corresponding diagram shown in Fig. S2(c) in the ESM. With 4 electrodes, the droplet mixing takes 160 s, while with 12 electrodes, the mixing process is reduced to only 60 s. The electric field duration is constant among the electrodes and as their number increases, the frequency of ion exchanges within the droplets also rises, greatly reducing droplet mixing time.

Apart from the microfluidic stage, droplet size, droplet type and concentration also significantly influence the mixing time. Experiments are conducted on a microdroplet manipulation platform with 8 electrodes and a 45° electrode central angle. As demonstrated in Fig. 5(e), for a total droplet volume of 10 μL, the mixing process is completed in only 60 s. However, when the droplet volume is increased to 60 μL, the mixing process takes 84 s. Figure 5(f)(i) examines the influence of droplet type and concentration on mixing time. At a droplet concentration of 62.5 mmol·L⁻¹, the complete mixing processes of NaOH with HCl and H₂SO₄ take 53 and 72 s, respectively. When the droplet concentration is increased to 200 mmol·L⁻¹, complete mixing takes 156 and 180 s, respectively. The mixing times for varying concentrations of HCl and H₂SO₄ are then fitted, the slopes of the fitting curves are $K(\text{HCl})$ and $K(\text{H}_2\text{SO}_4)$, respectively. The resulting curves show that $K(\text{HCl})$ which is 0.77988 is less than $K(\text{H}_2\text{SO}_4)$ which is 0.84388, which indicates that HCl mixing faster than H₂SO₄. The fitting accuracy of $R^2(\text{HCl})$ and $R^2(\text{H}_2\text{SO}_4)$ is 0.96609 and 0.94436 respectively, as displayed in Figs. 5(f)(ii) and 5(f)(iii). Different types of droplets contain varied ions. Under the same electric field force, these ions move at different speeds, leading to different complete droplet mixing times. Thus, the droplet type significantly affects the mixing time. In addition, the solution concentration also affects the charge transfer between the droplets and the FEP film, which also changes the force of droplets with different concentrations in the electric field to a certain extent, thus affecting the complete mixing time of droplet. The above results indicate that the SMDM based on the TENG design can rapidly manipulate droplets for mixing on a microdroplet manipulation platform. It introduces a novel method for TENG to realize green chemistry and compound synthesis in the microfluidics field.

2.6 Application demonstration of self-powered microdroplet manipulated system

The aforementioned experimental results demonstrate that SMDM exhibits great potential in the field of digital microfluidics. To enhance the method’s integration and portability, we developed a self-powered microdroplet manipulated system via TENG, as depicted in Fig. 6(a). The self-powered microdroplet manipulated system comprises a TENG, electric brush, switch circuit, microdroplet manipulation platform and a speed control system featuring a 1:12 gear ratio. To evaluate the self-powered microdroplet manipulated system’s performance in microdroplet manipulation, we conducted droplet mixing experiments via manual operation of the self-powered microdroplet manipulated system, as shown in Video S2 in the ESM. The self-powered microdroplet manipulated system has been experimentally proven to effectively perform the microdroplet manipulation. The specific processes of droplet splitting and mixing are respectively presented in Figs. 6(b) and 6(c). As evident in Fig. 6(d), the integration of TENG into micromechanical systems allows for the effective microdroplet manipulation, fostering the advancement and innovation in the realm of micro and nanodevices. The microdroplet manipulation system shows broad application prospects, including water quality detection in the field environment [56]; in the process of cell culture, the cells are separated from the solution and provide new nutrient solution for the cells; only require trace biological samples for blood testing and virus detection.

3 Conclusion

In conclusion, we proposed a SMDM via TENG, which allows for operations such as the split and mixed of microdroplets. Experimental results illustrate those droplets ranging from 2 to 630 μL can be successfully divided used the SMDM, with only 6.084 mW of power required for split a 60 μL droplet. Moreover, the TENG output voltage difference required for split droplets across different media was consistently within a 6.3% range. Our method effectively circumvents issues of cross-contamination frequently encountered in traditional techniques during the mixed process. For example, a 10 μL droplet with a concentration of 125 mmol·L⁻¹ can be completely mixed within 60 s, while a 30 μL droplet composed of 62.5 mmol·L⁻¹ HCl and NaOH can be mixed within 53 s. To streamline the method and foster a more integrated system, a self-powered microdroplet manipulated system was designed in this work for digital microfluidics. The self-powered microdroplet manipulated system boasted the advantages of being self-powered, flexible, portable and low-Joule heat. Utilizing TENG as a voltage source for digital microfluidics will greatly facilitate the portability of digital microfluidic devices and enhance the commercialization value of the digital microfluidics field.

4 Experimental section

4.1 The equipment manufacturing process

The TENG adopts a drum structure, which exhibits an overall dimension with an inner radius (r) of 75 mm and a height (H) of 110 mm. The triboelectric materials are FEP and copper respectively. The FEP sheet measuring 96 mm × 35 mm × 0.08 mm (length × width × thickness, $L \times W \times T$), one end of the FEP sheet

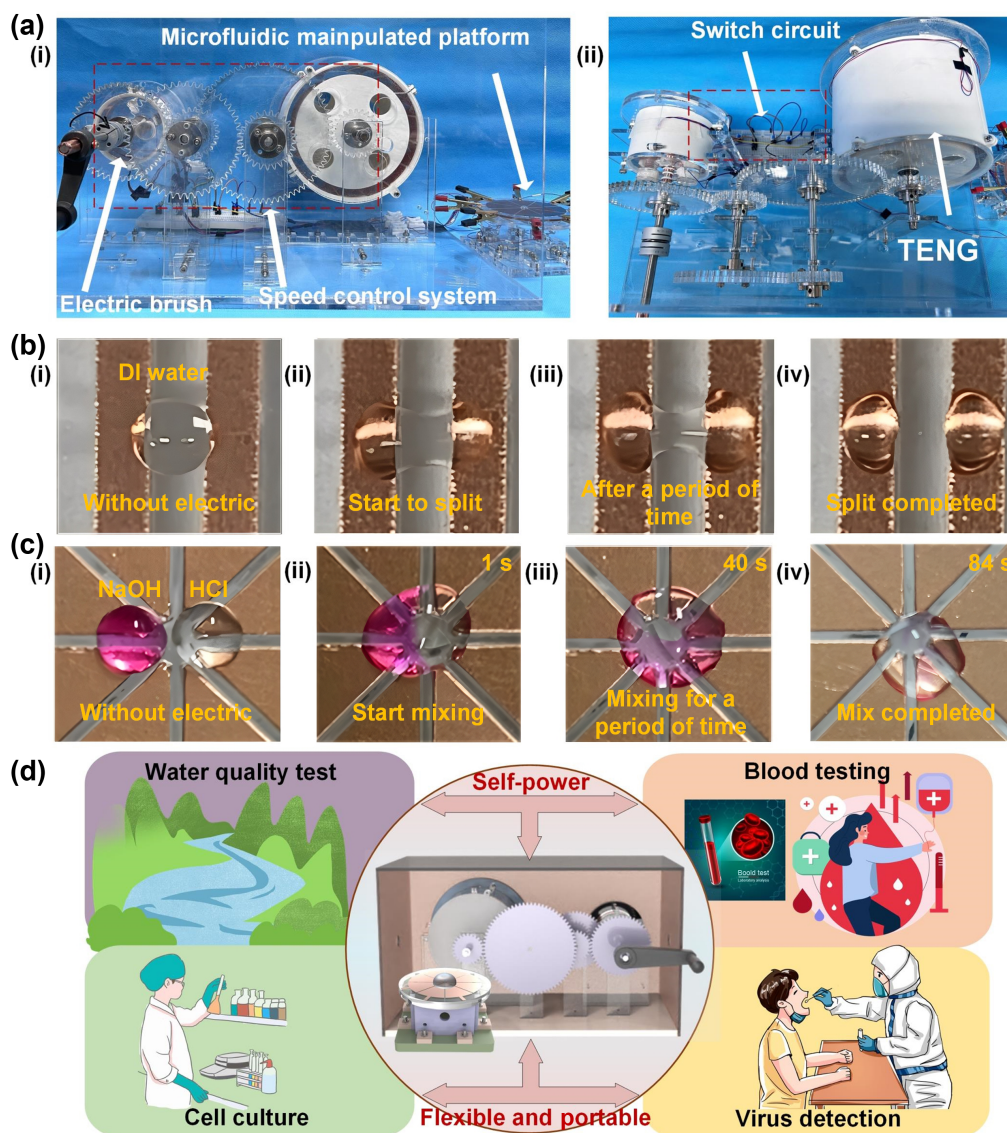


Figure 6 Application diagram of self-powered microdroplet manipulated system. (a) Microdroplet control device based on TENG (i) front view and (ii) top view. (b) manipulating droplet splitting, (c) manipulating droplet mixing. (d) Application prospect of self-powered microdroplet manipulated system.

is fixed on the rotor. The copper electrode is pasted on the inner wall of the drum. When the rotor rotates, the sliding friction between the FEP sheet and copper occurs. The electric brush follows suit with an r of 35 mm and a height (H) of 50 mm. The main structure of TENG and brush are manufactured using a three-dimensional (3D) printer (model: Raise 3D, E2, China), with polylactic acid (PLA) as the primary component. The blade electrodes of the electric brush, made of copper, have dimensions of 44 mm \times 60 mm \times 0.06 mm ($L \times W \times T$) and the internal electrodes of the brush, measure 20 mm \times 27 mm \times 0.06 mm ($L \times W \times T$). A layer of sponge glue (1 mm thick, 5 mm wide) is pasted on the rotating shaft of the brush and then a layer of electrode with the same area is covered on the sponge glue to complete the production of the conductive slip ring. For the microdroplet manipulation platform, 3 mm thick acrylic sheets are cut using a laser cutter (model: 31 degrees, 6090, China). The variable speed system employs gears with tooth counts of $Z_1 = 25$, $Z_2 = 50$ and $Z_3 = 75$ (Z_1 , Z_2 and Z_3 represent the number of teeth of the gear in the transmission system respectively), fabricated by cutting 5 mm

thick acrylic sheets in double layers.

4.2 Experimental measuring equipment

The TENG and electric brush are powered by a rotating motion actuator (model: Longshun, J-5718HBS401, China). The resulting current signals are examined using a programmable electrometer (model: Keithley 6514, USA) and collected by a data acquisition card (model: National Instruments, USB-6218, China). The output voltage is measured by a mixed domain oscilloscope (model: Tektronix, MDO34, USA) and the passive high voltage probe (model: Tektronix, P6015A, USA). The recorded data is subsequently outputted and displayed with the assistance of a computer and LabVIEW software. A contact angle measurement instrument (model: ZYKX, JC2000D, China) is employed to characterize the contact angle of the droplets.

Electronic Supplementary Material: Supplementary material (additional figures and videos) is available in the online version of this article at <https://doi.org/10.26599/NR.2025.94907128>.

Data availability

All data needed to support the conclusions in the paper are presented in the manuscript and the Electronic Supplementary Material. Additional data related to this paper may be requested from the corresponding author upon request.

Acknowledgements

The authors are grateful for the support from the National Natural Science Foundation of China (No. 52405052), the Open Foundation of the State Key Laboratory of Fluid Power and Mechatronic Systems (No. GZKF-202305), the Postdoctoral Fellowship Program (Grade B) of China Postdoctoral Science Foundation (No. GZB20230731), and the National Key R&D Project from Minister of Science and Technology (No. 2021YFA1201601).

Declaration of competing interest

The authors declare no conflict of interest. Author Zhong Lin Wang is the advisory board member of this journal, but he is not involved in the peer-review or decision of this article.

Author contribution statement

Q. G.: Conceptualization, investigation, writing – original draft, validation. Q. X.: Conceptualization, investigation, validation, writing – original draft. W. K. L.: Investigation, validation, editing. M. R. D.: Writing – review & editing, supervision. W. L.: Writing – review & editing, supervision. J. L. W.: Investigation, validation. X. J. C.: Validation, editing. H. Y. L.: Conceptualization, resources, writing – review & editing, supervision. Z. L. W.: Conceptualization, resources, writing – review & editing, supervision. T. H. C.: Conceptualization, resources, writing – review & editing, supervision.

Use of AI statement

None.

References

- Nge, P. N.; Rogers, C. I.; Woolley, A. T. Advances in microfluidic materials, functions, integration, and applications. *Chem. Rev.* **2013**, *113*, 2550–2583.
- Zhu, H. L.; Fohlerová, Z.; Pekárek, J.; Basova, E.; Neuzil, P. Recent advances in lab-on-a-chip technologies for viral diagnosis. *Biosens. Bioelectron.* **2020**, *153*, 112041.
- Wu, Q. R.; Liu, J. F.; Wang, X. H.; Feng, L. Y.; Wu, J. H.; Zhu, X. L.; Wen, W. J.; Gong, X. Q. Organ-on-a-chip: Recent breakthroughs and future prospects. *Biomed. Eng. Online* **2020**, *19*, 9.
- Knoška, J.; Adriano, L.; Awel, S.; Beyerlein, K. R.; Yefanov, O.; Oberthuer, D.; Peña Murillo, G. E.; Roth, N.; Sarrou, I.; Villanueva-Perez, P. et al. Ultracompact 3D microfluidics for time-resolved structural biology. *Nat. Commun.* **2020**, *11*, 657.
- Cho, S. K.; Moon, H.; Kim, C. J. Creating, transporting, cutting, and merging liquid droplets by electrowetting-based actuation for digital microfluidic circuits. *J. Microelectromech. Syst.* **2003**, *12*, 70–80.
- Teh, S. Y.; Lin, R.; Hung, L. H.; Lee, A. P. Droplet microfluidics. *Lab Chip* **2008**, *8*, 198–220.
- Sagar, N.; Bansal, S.; Sen, P. Open-chip droplet splitting in electrowetting. *Adv. Mater. Interfaces* **2022**, *9*, 2200240.
- Hu, Q. M.; Ren, Y. K.; Liu, W. Y.; Chen, X. M.; Tao, Y.; Jiang, H. Y. Fluid flow and mixing induced by AC continuous electrowetting of liquid metal droplet. *Micromachines* **2017**, *8*, 119.
- Kichatov, B.; Korshunov, A.; Sudakov, V.; Gubernov, V.; Golubkov, A.; Kiverin, A. Superfast active droplets as micromotors for locomotion of passive droplets and intensification of mixing. *ACS Appl. Mater. Interfaces* **2021**, *13*, 38877–38885.
- Ahmadi, F.; Samlali, K.; Vo, P. Q. N.; Shih, S. C. C. An integrated droplet-digital microfluidic system for on-demand droplet creation, mixing, incubation, and sorting. *Lab Chip* **2019**, *19*, 524–535.
- Xi, H. D.; Guo, W.; Leniart, M.; Chong, Z. Z.; Tan, S. H. AC electric field induced droplet deformation in a microfluidic T-junction. *Lab Chip* **2016**, *16*, 2982–2986.
- Hartmann, J.; Schür, M. T.; Hardt, S. Manipulation and control of droplets on surfaces in a homogeneous electric field. *Nat. Commun.* **2022**, *13*, 289.
- Li, B.; Vivacqua, V.; Ghadiri, M.; Sun, Z. Q.; Wang, Z. B.; Li, X. Y. Droplet deformation under pulsatile electric fields. *Chem. Eng. Res. Des.* **2017**, *127*, 180–188.
- Deng, Z. L.; Sun, M. M.; Yu, C. Electrohydrodynamic behaviors of droplet under a uniform direct current electric field. *Chin. Phys. B* **2020**, *29*, 034703.
- Feng, X. S.; Ren, Y. K.; Jiang, H. Y. Effect of the crossing-structure sequence on mixing performance within three-dimensional micromixers. *Biomicrofluidics* **2014**, *8*, 034106.
- Frommelt, T.; Kostur, M.; Wenzel-Schäfer, M.; Talkner, P.; Hänggi, P.; Wixforth, A. Microfluidic mixing via acoustically driven chaotic advection. *Phys. Rev. Lett.* **2008**, *100*, 034502.
- Ryu, K. S.; Shaikh, K.; Goluch, E.; Fan, Z. F.; Liu, C. Micro magnetic stir-bar mixer integrated with parylene microfluidic channels. *Lab Chip* **2004**, *4*, 608–613.
- Cui, K.; Zhao, Z. L.; Ma, L.; Liu, W. B.; Li, D. Y.; Ma, X. H. Effect of time-varying magnetic field on metal droplet profiles. *Indian J. Phys.* **2020**, *94*, 969–973.
- Collignon, S.; Friend, J.; Yeo, L. Planar microfluidic drop splitting and merging. *Lab Chip* **2015**, *15*, 1942–1951.
- Mandal, S.; Bandopadhyay, A.; Chakraborty, S. The effect of uniform electric field on the cross-stream migration of a drop in plane Poiseuille flow. *J. Fluid Mech.* **2016**, *809*, 726–774.
- Jia, Z. Q.; Chang, C. Y.; Hu, S. Y.; Li, J. H.; Ge, M. F.; Dong, W. F.; Ma, H. B. Artificial intelligence-enabled multipurpose smart detection in active-matrix electrowetting-on-dielectric digital microfluidics. *Microsyst. Nanoeng.* **2024**, *10*, 139.
- Guo, K. L.; Song, Z. R.; Zhou, J. L.; Shen, B.; Yan, B. Y.; Gu, Z.; Wang, H. F. An artificial intelligence-assisted digital microfluidic system for multistate droplet control. *Microsyst. Nanoeng.* **2024**, *10*, 138.
- Sun, G. J.; Yun, J. H.; Cheon, M. W. Parallel switch configuration for high voltage DC switching to secure PV power system safety. *Trans. Electr. Electron. Mater.* **2021**, *22*, 108–113.
- Haes Alhelou, H.; Siano, P. Special issue on advances and technologies in high voltage power systems operation, control, protection, and security. *Appl. Sci.* **2020**, *11*, 274.
- Qiao, M.; Liang, L. F.; Zu, J.; Hou, D. C.; Li, Z. J.; Zhang, B. A review of high-voltage integrated power device for AC/DC switching application. *Microelectron. Eng.* **2020**, *232*, 111416.
- Yakimov, A. S.; Denisov, I. A.; Bukatin, A. S.; Lukyanenko, K. A.; Belousov, K. I.; Kukhtevich, I. V.; Esimbekova, E. N.; Evstrapov, A. A.; Belobrov, P. I. Droplet microfluidic device for chemoenzymatic sensing. *Micromachines* **2022**, *13*, 1146.
- Fan, F. R.; Tian, Z. Q.; Lin Wang, Z. Flexible triboelectric generator. *Nano Energy* **2012**, *1*, 328–334.
- Lin, Z. M.; Zhang, B. B.; Guo, H. Y.; Wu, Z. Y.; Zou, H. Y.; Yang, J.; Wang, Z. L. Super-robust and frequency-multiplied triboelectric nanogenerator for efficient harvesting water and wind energy. *Nano Energy* **2019**, *64*, 103908.
- Li, A. Y.; Zi, Y. L.; Guo, H. Y.; Wang, Z. L.; Fernández, F. M.

- Triboelectric nanogenerators for sensitive nano-Coulomb molecular mass spectrometry. *Nat. Nanotechnol.* **2017**, *12*, 481–487.
- [30] Cheng, L.; Xu, Q.; Zheng, Y. B.; Jia, X. F.; Qin, Y. A self-improving triboelectric nanogenerator with improved charge density and increased charge accumulation speed. *Nat. Commun.* **2018**, *9*, 3773.
- [31] Guo, H. Y.; Chen, J.; Wang, L. F.; Wang, A. C.; Li, Y. F.; An, C. H.; He, J. H.; Hu, C. G.; Hsiao, V. K. S.; Wang, Z. L. A highly efficient triboelectric negative air ion generator. *Nat. Sustain.* **2020**, *4*, 147–153.
- [32] Yu, J. J.; Wei, X. X.; Guo, Y. C.; Zhang, Z. W.; Rui, P. S.; Zhao, Y.; Zhang, W.; Shi, S. W.; Wang, P. H. Self-powered droplet manipulation system for microfluidics based on triboelectric nanogenerator harvesting rotary energy. *Lab Chip* **2021**, *21*, 284–295.
- [33] Nie, J. H.; Ren, Z. W.; Shao, J. J.; Deng, C. R.; Xu, L.; Chen, X. Y.; Li, M. C.; Wang, Z. L. Self-powered microfluidic transport system based on triboelectric nanogenerator and electrowetting technique. *ACS Nano* **2018**, *12*, 1491–1499.
- [34] Zhou, J.; Tao, Y.; Liu, W. Y.; Sun, H. Z.; Wu, W. L.; Song, C. L.; Xue, R.; Jiang, T. Y.; Jiang, H. Y.; Ren, Y. K. Self-powered AC electrokinetic microfluidic system based on triboelectric nanogenerator. *Nano Energy* **2021**, *89*, 106451.
- [35] Sun, J. F.; Zhang, L. J.; Li, Z. J.; Tang, Q.; Chen, J.; Huang, Y. Z.; Hu, C. G.; Guo, H. Y.; Peng, Y.; Wang, Z. L. A mobile and self-powered micro-flow pump based on triboelectricity driven electroosmosis. *Adv. Mater.* **2021**, *33*, 2102765.
- [36] Li, X. Y.; Tat, T.; Chen, J. Triboelectric nanogenerators for self-powered drug delivery. *Trends Chem.* **2021**, *3*, 765–778.
- [37] Li, X. H.; Yeh, M. H.; Lin, Z. H.; Guo, H. Y.; Yang, P. K.; Wang, J.; Wang, S. H.; Yu, R. M.; Zhang, T. J.; Wang, Z. L. Self-powered triboelectric nanosensor for microfluidics and cavity-confined solution chemistry. *ACS Nano* **2015**, *9*, 11056–11063.
- [38] Xu, J.; Yin, J. Y.; Fang, Y. S.; Xiao, X.; Zou, Y. J.; Wang, S. L.; Chen, J. Deep learning assisted ternary electrification layered triboelectric membrane sensor for self-powered home security. *Nano Energy* **2023**, *113*, 108524.
- [39] Zhao, X.; Sun, Z. D.; Lee, C. Augmented tactile perception of robotic fingers enabled by AI-enhanced triboelectric multimodal sensors. *Adv. Funct. Mater.*, in press, DOI: [10.1002/adfm.202409558](https://doi.org/10.1002/adfm.202409558).
- [40] Zhang, Z. X.; Guo, X. G.; Lee, C. Advances in olfactory augmented virtual reality towards future metaverse applications. *Nat. Commun.* **2024**, *15*, 6465.
- [41] Zhang, Z. X.; Wang, L. W.; Lee, C. Recent advances in artificial intelligence sensors. *Adv. Sens. Res.* **2023**, *2*, 2200072.
- [42] Zhang, Z. X.; Wen, F.; Sun, Z. D.; Guo, X. G.; He, T. Y. Y.; Lee, C. Artificial intelligence-enabled sensing technologies in the 5G/Internet of Things era: From virtual reality/augmented reality to the digital twin. *Adv. Intell. Syst.* **2022**, *4*, 2100228.
- [43] Kwak, W.; Yin, J. Y.; Wang, S. L.; Chen, J. Advances in triboelectric nanogenerators for self-powered wearable respiratory monitoring. *FlexMat* **2024**, *1*, 5–22.
- [44] Yang, Y. Q.; Guo, X. G.; Zhu, M. L.; Sun, Z. D.; Zhang, Z. X.; He, T. Y. Y.; Lee, C. Triboelectric nanogenerator enabled wearable sensors and electronics for sustainable internet of things integrated green earth. *Adv. Energy Mater.* **2023**, *13*, 2203040.
- [45] Lei, R.; Shi, Y. X.; Ding, Y. F.; Nie, J. H.; Li, S. Y.; Wang, F.; Zhai, H.; Chen, X. Y.; Wang, Z. L. Sustainable high-voltage source based on triboelectric nanogenerator with a charge accumulation strategy. *Energy Environ. Sci.* **2020**, *13*, 2178–2190.
- [46] Zeng, S. J.; Liu, X.; Xie, H.; Lin, B. C. Basic technologies for droplet microfluidics. *Top. Curr. Chem.* **2011**, *304*, 69–90.
- [47] Wu, B. D.; Zhou, J. Q.; Guo, Y. Y.; Zhu, R.; Wang, D.; An, C. W.; Wang, J. Y. Preparation of HMX/TATB spherical composite explosive by droplet microfluidic technology. *Def. Technol.* **2023**, *21*, 62–72.
- [48] Peretzki, A. J.; Belder, D. On-chip integration of normal phase high-performance liquid chromatography and droplet microfluidics introducing ethylene glycol as polar continuous phase for the compartmentalization of *n*-heptane eluents. *J. Chromatogr. A* **2020**, *1612*, 460653.
- [49] Zhou, J.; Tao, Y.; Xue, R.; Ren, Y. K. A self-powered dielectrophoretic microparticle manipulation platform based on a triboelectric nanogenerator. *Adv. Mater.* **2023**, *35*, 2207093.
- [50] Chen, Z. K.; Kheiri, S.; Young, E. W. K.; Kumacheva, E. Trends in droplet microfluidics: From droplet generation to biomedical applications. *Langmuir* **2022**, *38*, 6233–6248.
- [51] Zhu, J. L.; Wang, Z.; Li, R. N.; Liu, S. Experimental research on the disruptive evaporation and the motion characteristics of secondary droplets for emulsified biodiesel with a suspended droplet configuration. *ACS Omega* **2021**, *6*, 17848–17860.
- [52] Donau, C.; Boekhoven, J. The chemistry of chemically fueled droplets. *Trends Chem.* **2023**, *5*, 45–60.
- [53] Meredith, C. H.; Castonguay, A. C.; Chiu, Y. J.; Brooks, A. M.; Moerman, P. G.; Torab, P.; Wong, P. K.; Sen, A.; Velegol, D.; Zarzar, L. D. Chemical design of self-propelled Janus droplets. *Matter* **2022**, *5*, 616–633.
- [54] Cunningham, M. H.; Frost, D. L. Fragmentation of a molten metal droplet in an ambient water flow. *Front. Phys.* **2023**, *11*, 1171267.
- [55] Chen, L. D. Effects of ambient temperature and humidity on droplet lifetime—A perspective of exhalation sneeze droplets with COVID-19 virus transmission. *Int. J. Hyg. Environ. Health* **2020**, *229*, 113568.
- [56] Wu, Z. Y.; Wang, J. Q.; Bian, C.; Tong, J. H.; Xia, S. H. A MEMS-based multi-parameter integrated chip and its portable system for water quality detection. *Micromachines* **2020**, *11*, 63.



This is an open access article under the terms of the Creative Commons Attribution 4.0 International License (CC BY 4.0, <https://creativecommons.org/licenses/by/4.0/>).

© The Author(s) 2025. Published by Tsinghua University Press.